

Martian World Model: Controllable Video Synthesis with Physically Accurate 3D Reconstructions

Longfei Li¹, Zhiwen Fan^{2,*}, Wenyan Cong², Xinhang Liu³,
Yuyang Yin¹, Matt Foutter⁴, Panwang Pan⁵, Chenyu You⁶, Yue Wang^{7,8},
Zhangyang Wang², Yao Zhao¹, Marco Pavone^{4,8}, Yunchao Wei^{1†}

¹BJTU ²UT Austin ³HKUST ⁴Stanford University ⁵XMU ⁶SBU ⁷USC ⁸NVIDIA

Project Website: <https://marsgenai.github.io>

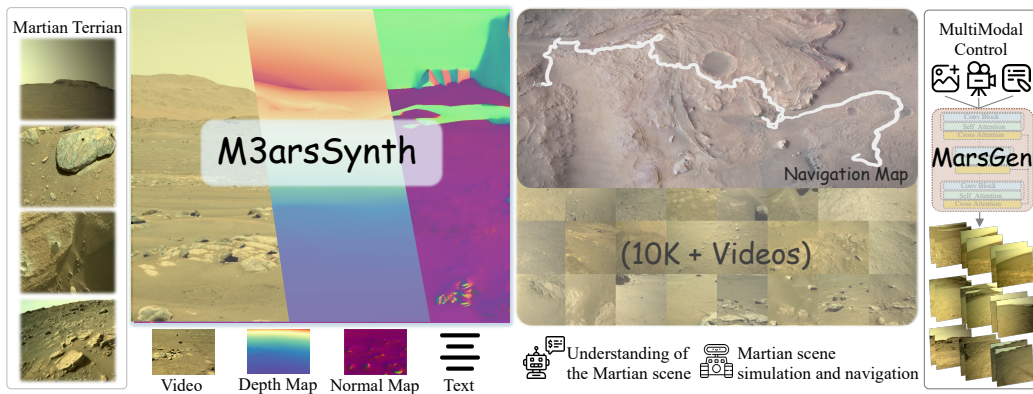


Figure 1: **Overview of the M3arsSynth data engine and MarsGen video generator.** The **M3arsSynth** engine processes NASA stereo navigation imagery into a versatile multimodal Mars dataset comprising video, depth/normal maps (from 3D reconstructions), and text descriptions. These outputs advance Mars scene generation and simulation for mission rehearsal and robotic navigation.

Abstract

Synthesizing realistic Martian landscape videos is crucial for mission rehearsal and robotic simulation. However, this task poses unique challenges due to the scarcity of high-quality Martian data and the significant domain gap between Martian and terrestrial imagery. To address these challenges, we propose a holistic solution composed of two key components: 1) A data curation pipeline *Multimodal Mars Synthesis (M3arsSynth)*, which reconstructs 3D Martian environments from real stereo navigation images, sourced from NASA’s Planetary Data System (PDS), and renders high-fidelity multiview 3D video sequences. 2) A Martian terrain video generator, *MarsGen*, which synthesizes novel videos visually realistic and geometrically consistent with the 3D structure encoded in the data. Our M3arsSynth engine spans a wide range of Martian terrains and acquisition dates, enabling the generation of physically accurate 3D surface models at metric-scale resolution. MarsGen, fine-tuned on M3arsSynth data, synthesizes videos conditioned on an initial image frame and, optionally, camera trajectories or textual prompts, allowing for video generation in novel environments. Experimental results show that our approach outperforms video synthesis models trained on terrestrial datasets, achieving superior visual fidelity and 3D structural consistency.

*Z. Fan is the Project Lead

†Y. Wei is the Corresponding Author

1 Introduction

The advancement of space exploration is critically dependent on the development of robust robotic systems and operational procedures Gao and Chien (2017) tailored to diverse extraterrestrial environments. A major challenge across such domains is the lack of platforms capable of synthesizing realistic and dynamic data. This limitation hinders autonomous mission planning Maurette (2003), operational rehearsal Wright et al. (2005), rover navigation, and the execution of complex robotic tasks Huntsberger et al. (2000); Mathers et al. (2012). Current publicly available extraterrestrial imagery, for example from NASA’s Martian rovers such as Curiosity and Perseverance—is typically provided as static stereo pairs captured from discrete and sparsely distributed viewpoints. The quality of these images is also affected by the interplanetary bandwidth limitations Goldstein (1968) and operational constraints. As a result, reconstruction of photorealistic 3D environments from such sparse and constrained imagery, a common challenge in planetary datasets, remains an obstacle.

Recent advances in video synthesis Brooks et al. (2024); Kong et al. (2024); Jin et al. (2024) offer promising avenues to mitigate these challenges. However, training an effective video generation model conditioned on sparse Martian imagery or reconstructed 3D models remains difficult. Most existing models Yang et al. (2024); Wang et al. (2025a), which are typically trained on large-scale terrestrial datasets, struggle to generalize to the Martian domain due to the substantial domain gap. In addition, the challenges inherent to 3D reconstruction on Martian data often result in geometric models with insufficient accuracy, making it difficult to support high-fidelity, 3D-consistent video synthesis from such limited inputs.

To bridge this gap, we introduce a holistic solution for the synthesis of realistic Martian landscape 3D videos. We first propose **Multimodal Mars Synthesis (M3arsSynth)**, a data curation framework. M3arsSynth processes sparse and photometrically inconsistent stereo navigation images, sourced from NASA’s Planetary Data System (PDS)³. Leveraging the strong generalization capabilities of geometric foundation models, it achieves robust 3D scene reconstruction as a critical intermediate step. This process allows for the creation of physics-accurate 3D surface models at metric-scale resolution, which form the basis for rendering high-fidelity 3D video sequences. The principal output of M3arsSynth is a large-scale, versatile multimodal dataset. This dataset includes synthesized videos, corresponding camera motion trajectories, detailed geometric information such as depth maps, and associated textual descriptions, all designed for diverse Martian applications. The second component of our solution is **MarsGen**, a video-based Martian terrain generator. MarsGen utilizes the rich dataset produced by M3arsSynth along with other multimodal conditioning inputs (such as an initial image frame, specified camera trajectories, or textual prompts) to accurately synthesize novel, 3D-consistent video frames and dynamic environments, enabling the controllable generation of new Martian scenarios not present in the original rover data.

Experimental results demonstrate that our unified solution significantly surpasses existing Earth-trained video synthesis approaches, encompassing both open-source and closed-source alternatives. Our method achieves superior visual quality in the generated Martian videos, robust 3D consistency across frames, and enhanced camera controllability, offering a substantial improvement for realistic simulation. Our primary contributions are:

- We introduce M3arsSynth, a multimodal data engine that transforms challenging rover-captured stereo navigation imagery into high-quality assets for synthesizing controllable video for Mars missions. By leveraging geometric foundation models, M3arsSynth creates metric-scale 3D environments, effectively addressing critical issues such as sparse-view coverage and photometric inconsistencies to produce over 10K physically accurate 3D Martian surface models.
- Our work enables controllable video generation of Martian terrain, MarsGen, starting from a single-view image input and conditioned on camera poses or text prompts, yielding photorealistic and 3D-consistent video sequences.
- We evaluate our generated controllable video across key metrics, including visual fidelity, our proposed 3D video consistency, and camera controllability. Our approach significantly outperforms models trained primarily on terrestrial data, demonstrating its strong potential for future data-driven robotic simulation.

³<https://pds-imaging.jpl.nasa.gov/beta/archive-explorer>

2 Related works

Planetary Environment Simulation. Prior efforts in simulating planetary environments Jain et al. (2003); Tian et al. (2024) have focused on enhancing the interpretation and interaction with Martian data. Approaches include Mixed Reality (MR) technologies Mahmood et al. (2019); Memarsadeghi and Varshney (2020), such as those developed by NASA JPL’s Operations Lab and Microsoft Abercrombie et al. (2017); Beaton et al. (2020), enabling immersive exploration of 3D terrain models from rover data. Additionally, 3D reconstruction techniques like the MaRF Giusti et al. (2022) framework, which employs Neural Radiance Fields (NeRF) Mildenhall et al. (2021) for continuous volumetric representations from sparse images, have improved visualization from novel viewpoints. However, the MaRF framework is notably limited, having been demonstrated in different 3D environments. More broadly, these existing technologies often require high-quality, consistent visual data and exhibit limitations in scalability and adaptability. Our approach addresses these challenges by employing video generation models trained on a dedicated video dataset produced by our specialized data processing pipeline.

3D Modeling from Sparse Views. Reconstructing 3D scenes from sparse views Chen and Wang (2024) is a significant challenge. NeRF and 3DGS Kerbl et al. (2023) typically demand hundreds of images and rely on the Structure-from-Motion (SfM) Schönberger and Frahm (2016) approach (e.g., COLMAP Schonberger and Frahm (2016)). To address this, some works leverage priors by pre-training on large datasets Chen et al. (2021); Johari et al. (2022); Yu et al. (2021); Chibane et al. (2021); Jang and Agapito (2021) or by applying regularization during NeRF optimization Wang et al. (2023); Roessle et al. (2023); Seo et al. (2023); Somraj et al. (2023); Somraj and Soundararajan (2023); Wynn and Turmukhambetov (2023); Liu et al. (2024). To mitigate the overfitting to input views in 3DGS, FSGS Zhu et al. (2024) and SparseGS Xiong (2024) incorporate external priors from depth estimator with the optimization process. Others, like InstantSplat Fan et al. (2024), utilize powerful 3D reconstruction models Leroy et al. (2024) to acquire accurate camera poses and initial geometries. However, robust sparse-view reconstruction remains an open problem, particularly in challenging environments such as the Martian surface, which exhibit textureless areas, repetitive patterns, and photometric variations. Our method addresses this gap by integrating a 3D geometric foundation model for initial geometric estimation with a specialized pipeline for refinement and neural scene representation from sparse stereo imagery, facilitating high-quality multimodal data synthesis.

Conditional Generative Models. Recent text-to-video models Yang et al. (2024); Kong et al. (2024); Wang et al. (2025a); Blattmann et al. (2023) based on Diffusion Transformers (DiTs) Peebles and Xie (2023) leverage the scalability of transformers, typically employing text encoders Radford et al. (2021); Raffel et al. (2020), a 3D-VAE Yu et al. (2023); Yang et al. (2024) for video compression and tokenization, and a transformer generator that processes flattened video and text tokens. These architectures model spatiotemporal and textual information through global attention mechanisms or separate self- and cross-attention, leading to significant improvements in generation duration and temporal consistency. View-controllable video generation Wang et al. (2024c); He et al. (2024); Liang et al. (2024); Bahmani et al. (2024); Yu et al. (2024), which is crucial for immersive simulations, has seen efforts to integrate camera control into pretrained models. However, these methods, predominantly trained on standard terrestrial datasets, often exhibit difficulties with 3D consistency when applied to out-of-domain environments like Mars. In contrast, our work utilizes the M3arsSynth dataset, specifically curated with rich 3D geometric information, to train MarsGen, enabling physically plausible and precisely controllable Martian simulations with enhanced 3D consistency.

3 Multimodal Mars Synthesis

We establish the M3arsSynth dataset from curated rover stereo image from NASA PDS. To render a large-scale multimodal dataset suitable for training generative simulators, we leverage robust, pre-trained vision foundation models to capture Martian visual cues and compensate for the lack of Mars-specific priors. In this section, Sec. 3.1 first describes the source data acquisition and preprocessing steps. Sec. 3.2 then outlines the metric-aware 3D reconstruction process. Sec. 3.3 details the synthesis of multimodal data, and summarizes the overall structure of the dataset. Finally, Sec. 3.4 explains the proposed 3D consistency metrics for evaluating generated video sequences.

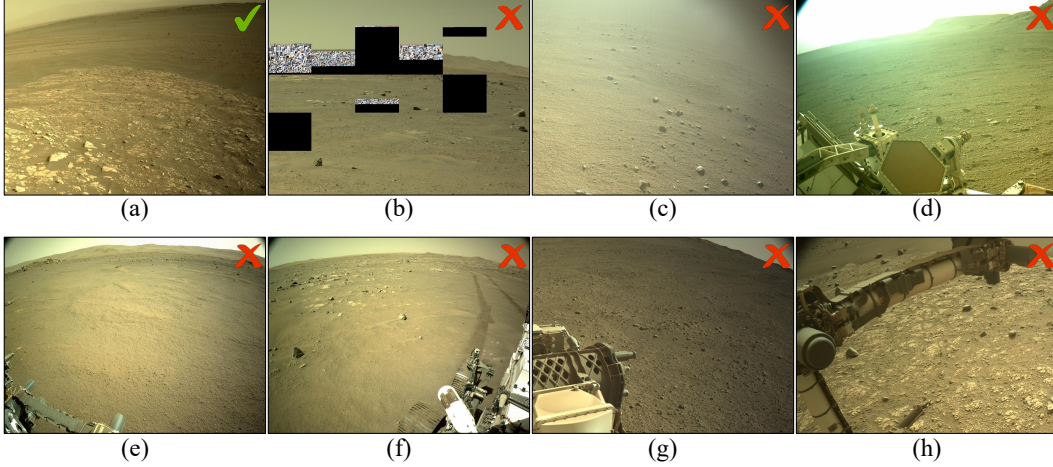


Figure 2: **Data Filtering Examples for Martian 3D Reconstruction.** Image (a) represents a clear, usable Martian terrain view, serving as a quality benchmark. In contrast, images (b)-(h) illustrate common defects that lead to data exclusion for high-quality reconstruction, including: (b) extensive missing data blocks or pixelation/mosaic artifacts (indicative of data corruption or severe compression); (c) significant image blur or out-of-focus areas; (d) scenes with extreme overexposure or harsh lighting conditions; and (e)-(h) views obstructed by spacecraft components.

3.1 Martian Stereo Image Acquisition and Preprocessing

Raw stereo image pairs captured by Martian rovers are sourced from PDS. This initial dataset, however, exhibits several deficiencies, including small thumbnail images, grayscale images, and duplicate captures made with different color filters, rendering it unsuitable for direct application. To address these issues, an automated filtering pipeline is implemented. This pipeline is designed to systematically remove these types of deficient data:

Systematic Data Filtering Strategy. A multi-stage filtering pipeline ensures visual dataset integrity by systematically addressing imperfections. Firstly, *low-resolution and grayscale images are eliminated*. Thumbnails are discarded based on size heuristics. Grayscale images are removed based on low RGB channel variance. Secondly, *redundant content is excluded using perceptual hashing* Zaver (2010). This technique employs hash codes and Hamming distances to identify and remove near-duplicates captured under varied imaging conditions, preserving semantic diversity. Thirdly, *blurry and low-sharpness images are rejected*. A sharpness filter using Laplacian variance Bansal et al. (2016) discards images with low edge contrast to maintain geometric and photometric quality, which is vital for tasks like stereo reconstruction. Finally, *frames exhibiting anomalous color distributions are filtered out*. Irrelevant frames (e.g., obscured, malfunctions), identified by skewed or flat color intensity histograms, are removed to ensure clear, terrain-focused scenes for robust surface representation learning. (See Appendix A.1 for details.)

Semi-Automated Refinement. To address complex visual artifacts like hardware occlusions and unfavorable lighting that degrade reconstruction quality (see Fig. 2), we employ a semi-automated refinement process. This step supplements manual image verification with Grounded-SAM Ren et al. (2024), which we use to generate segmentation masks identifying non-terrain objects based on textual prompts. These masks guide human annotators to efficiently identify and discard compromised image data. The result is a curated collection of images with high visual integrity, providing a reliable foundation for robust stereo reconstruction. Further details on this preprocessing are provided in Appendix A.2.

3.2 Neural 3D Reconstruction from Navigation Stereo Cameras

Dense Martian 3D reconstruction poses unique challenges compared to terrestrial scenes, stemming from the planet’s often texture-poor terrain and the inherent scarcity of observational data.

Camera Calibration. Our 3D reconstruction pipeline operates on the standard pinhole camera model Hartley (2003) and therefore requires the corresponding camera parameters. However, the PDS metadata accompanying our dataset lacks these crucial calibration parameters. To address this limitation, we infer the necessary parameters directly from the images. We employ the Visual Geometry Grounded Transformer (VGGT) Wang et al. (2025b), a feed-forward neural network

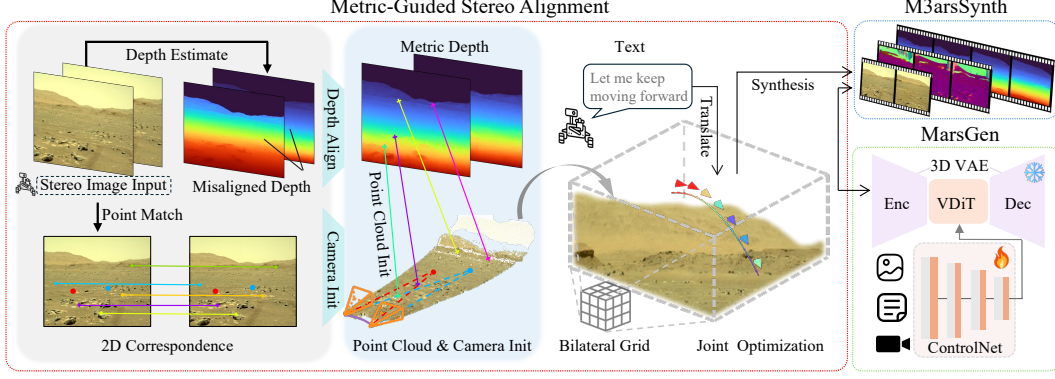


Figure 3: **Overview of the M3arsSynth dataset construction and conditional video generation through MarsGen.** The red box outlines the data curation pipeline, the green box shows the obtained M3arsSynth dataset, and the blue box details our MarsGen model. We process stereo image pairs using a metric-aware foundation model and solve the Perspective-n-Point (PnP) Lepetit et al. (2009) problem to reconstruct metric-scale 3D Martian scenes. Subsequently, video frames rendered from these scenes, together with text prompts and encoded camera trajectories, are then used to condition a Video Diffusion Transformer, enabling the synthesis of novel and controllable Martian video sequences.

designed to infer key 3D scene attributes from input views. Our empirical evaluations confirm that VGGT reliably predicts the camera intrinsics from the input stereo images, providing the essential parameters for subsequent reconstruction tasks.

Dense 3D Geometry Initialization. After obtaining camera intrinsics, we estimate metric depth maps using a pretrained monocular depth estimation network Hu et al. (2024) to construct dense 3D geometry. Each depth map is then back-projected using the inverse intrinsic matrix K^{-1} to transform each pixel (u, v) with depth d into a 3D point in the corresponding camera coordinate system: $P_c = d \cdot K^{-1}[u, v, 1]^T$. This process yields initial per-view point clouds where each pixel has a direct 3D correspondence within its respective camera frame, providing a dense geometry initialization.

Relative Pose Estimation and Geometric Refinement. To establish a coherent 3D model, we recover the relative camera extrinsics between the stereo images. We formulate this task as a Perspective-n-Point (PnP) Li et al. (2012) optimization, as PnP computes the camera pose from a set of 3D points and their corresponding 2D image projections. This approach utilizes robust 2D feature correspondences $\mathbf{p}_1 \leftrightarrow \mathbf{p}_2$ between the stereo image pair, which are detected using the Generalizable Image Matcher (GIM) Shen et al. (2024). GIM’s notable generalization capability stems from its training on extensive and varied internet video data (approximately 180,000 image pairs from 50 hours of video) and its sophisticated self-training framework. This enables robust matching across diverse conditions and often surpasses traditional methods that rely on less diverse datasets or failure-prone 3D reconstruction processes Shen et al. (2024). Here, \mathbf{p}_1 and \mathbf{p}_2 represent matched pixel coordinate vectors in the left and right views, respectively. Initial depth estimates from the monocular network are used to back-project points \mathbf{p}_1 into 3D space, yielding a set of 3D points \mathbf{P}_1 . Given the known camera intrinsics K , these 2D-3D correspondences (formed by $\mathbf{P}_{1,i}$ and their corresponding $\mathbf{p}_{2,i}$) facilitate the estimation of the relative camera pose.

The PnP solver estimates the rotation R_{rel} and translation \mathbf{t}_{rel} that best align the 3D points $\mathbf{P}_{1,i}$ with their corresponding 2D projections $\mathbf{p}_{2,i}$ in the second view by minimizing the reprojection error:

$$\min_{R_{\text{rel}}, \mathbf{t}_{\text{rel}}} \sum_i \|\mathbf{p}_{2,i} - \pi(K[R_{\text{rel}} | \mathbf{t}_{\text{rel}}]\mathbf{P}_{1,i})\|^2, \quad (1)$$

where π denotes the perspective projection from the 3D camera coordinates to the 2D pixel space. The initial geometry derived from the monocular depth estimation may exhibit inconsistencies, particularly in scale across views. To ensure a coherent 3D reconstruction, we apply a depth rescaling step after pose estimation. Specifically, we first back-project the depth map D_0 from view 0 to reconstruct its corresponding 3D point cloud P_0 . Then we project it onto view 1’s image plane. This warping process yields a new sparse depth map $D'_{0 \rightarrow 1}$ and a Boolean mask M_{sparse} , indicating valid

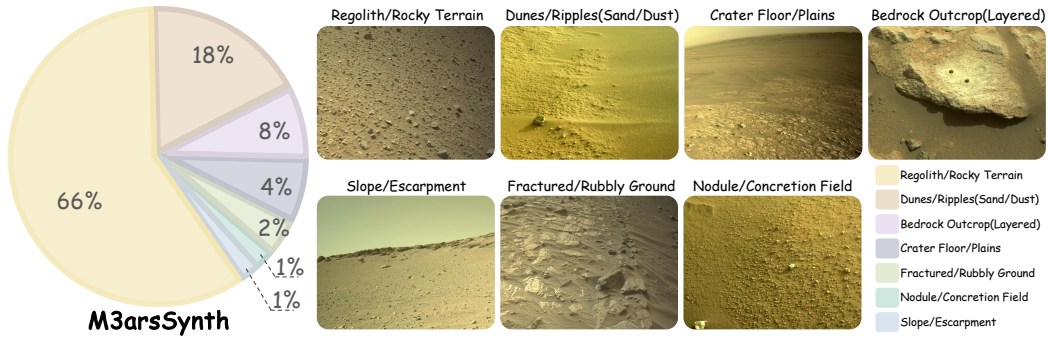


Figure 4: Distribution of primary terrain types within the M3arsSynth dataset, showcasing the diversity of Martian environments covered. The left chart indicates the percentage of scenes predominantly featuring each terrain type, with visual examples illustrating the various terrain categories.

projection areas in view 1. The depth value d'_1 is stored in $D'_{0 \rightarrow 1}$ at the projected pixel coordinates $(u'_1/d'_1, v'_1/d'_1)$.

$$P_0 = D_0(p_0) \cdot K_0^{-1} \begin{bmatrix} u_0 \\ v_0 \\ 1 \end{bmatrix}$$

$$\begin{bmatrix} u'_1 \\ v'_1 \\ d'_1 \end{bmatrix} = K_1(RP_0 + t)$$

Then, we align the original monocular depth map of view 1 D_1 , with the warped sparse depth map $D'_{0 \rightarrow 1}$. We solve a least-squares regression problem only within the valid region defined by the mask M_{sparse} .

$$\min_{s,b} \sum_{(u,v) \in M_{sparse}} (s \cdot D_1(u,v) + b - D'_{0 \rightarrow 1}(u,v))^2$$

This estimated (s, b) are then used to adjust the depth map of the first view (i.e., $d_{1,j}^{\text{adjusted}} = s \cdot d_{1,j} + b$) to better match the scale and offset of the second view's depth map, or vice-versa, thereby enhancing geometric consistency.

3D Gaussian Splatting for Photorealistic Scene Modeling. Using the camera parameters and dense point cloud from prior stages, we optimize a 3DGS Kerbl et al. (2023); Huang et al. (2024) representation, initializing Gaussian primitives directly from the per-pixel points Fan et al. (2024). The optimization combines a photometric loss with a depth regularization loss Xu et al. (2025); Xiong (2024); Li et al. (2024); Kerbl et al. (2024) that leverages our derived per-pixel correspondences to enforce geometric consistency. To mitigate significant appearance variations between Martian stereo pairs, often caused by differing camera settings or lighting, we integrate a bilateral grid Wang et al. (2024b) into the process. Specifically, our implementation is based on gsplat Ye et al. (2025). We apply a per-view 3D bilateral grid as a differentiable post-processing layer to the rendered image, which models view-dependent effects. This grid is jointly optimized with the Gaussian parameters by minimizing the difference between the post-processed render and the corresponding training view, while a total variation loss is used to regularize the grid for smoothness. Furthermore, since standard k-nearest neighbor initialization can produce overly large Gaussian scales and degrade depth accuracy, we adopt a modified strategy Cong et al. (2025) where scale is determined by the nearest point along the depth axis.

$$\text{scale}(P_w) = d'_{\min}(P_w) / f_{\text{avg}}$$

3.3 Multimodal Martian Dataset Creation

Upon obtaining an optimized neural scene representation for a Martian scene, we sample a diverse set of virtual camera trajectories, denoted $\mathcal{M}_{\text{traj}}$, along which video sequences are rendered:

$$\mathcal{M}_{\text{traj}} = \left\{ T_t = \begin{pmatrix} \mathbf{R}_t & \mathbf{T}_t \\ \mathbf{0}_{1 \times 3} & 1 \end{pmatrix} \in SE(3) \mid t = 1, \dots, N \right\} \quad (2)$$

where each transformation T_t defines the 6-DOF camera pose at timestamp t , comprising a rotation \mathbf{R}_t and a translation \mathbf{T}_t . Canonical trajectory types are defined, encompassing diverse motion profiles. Their spatial extent is adapted to the scene geometry through depth-adaptive scaling: trajectories are

contracted for near-field regions to capture fine details and expanded for far-field regions to facilitate wider movements. Further details regarding the specific parameters and generation process for these trajectories are provided in the Supplementary Material.

Video, Normal, Trajectory, Depth, Text. From a set of adaptively scaled camera trajectories, we generate a comprehensive multimodal dataset. Novel view videos, accompanied by their corresponding depth and normal maps, are produced by rendering the scene along these trajectories. The Trajectory modality encompasses the precise 6-DOF pose parameters for each frame (T_t), from which textual descriptions of camera motion are subsequently derived. To capture scene content, we further generate textual captions by applying a Vision Language Model (VLM) OpenAI (2024) to the rendered videos. This procedure results in a rich dataset comprising visual, geometric, and textual modalities, all structured around the foundational camera trajectories.

Dataset Structure. The resulting M3arsSynth dataset consists of a diverse set of distinct Martian scenes, each reconstructed and rendered from an optimized neural scene representation. For each scene, we generate multiple video sequences, each simulating a unique virtual camera trajectory. These sequences are temporally structured and provide rich, time-aligned multimodal information. Specifically, each sequence contains: (i) synthesized RGB frames rendered from novel viewpoints, (ii) precise 6-DOF camera poses corresponding to each frame, (iii) natural language descriptions detailing both the visual content and camera motion characteristics, and (iv) corresponding per-frame geometric outputs, including depth maps and optionally surface normal maps.

3.4 Metrics Evaluating 3D Consistency

To assess the 3D consistency of video sequences generated by our MarsGen model (trained on the M3arsSynth dataset), we employ the *2D Warp Error* metric Wang et al. (2024a).

The 2D Warp Error measures the internal geometric consistency of the 3D structure implicitly represented in the generated video frames. Specifically, this metric evaluates how accurately 3D points, inferred from each generated frame, are reprojected onto other frames or consistently within the same frame. The closer these reprojected points align with their corresponding expected 2D locations (e.g., on a canonical grid), the more consistent the underlying geometry is considered. This evaluation comprises two main components:

Self-Reprojection Consistency. For each generated frame i within a sequence, an associated 3D point cloud $\mathcal{P}_i^{(c)}$ (composed of points $\mathbf{p}_j^{(c)}$) in its local camera coordinate system, along with the camera intrinsic matrix K_i , is typically inferred using a geometric perception model applied to that frame. Each 3D point $\mathbf{p}_j^{(c)} \in \mathcal{P}_i^{(c)}$ is then projected onto the 2D image plane of frame i using K_i , resulting in reprojected pixel coordinates $\mathbf{x}_{\text{reproj},j}$. The self-reprojection consistency for frame i is computed as the mean squared Euclidean distance between these reprojected coordinates and their expected positions on a canonical 2D sampling grid:

$$L_{\text{self-reproj},i} = \frac{1}{M} \sum_j \|\mathbf{x}_{\text{reproj},j} - \mathbf{x}_{\text{gtgrid},j}\|_2^2, \quad (3)$$

where M denotes the number of points in $\mathcal{P}_i^{(c)}$, and $\mathbf{x}_{\text{gtgrid},j}$ is the source grid location of point j .

Cross-View Reprojection Consistency. To evaluate geometric consistency across different viewpoints, we measure the cross-frame reprojection between frame i and another frame k from the same sequence. First, we estimate the 3D point cloud $\mathcal{P}_k^{(c)}$ (composed of points $\mathbf{p}_{j'}^{(c)}$) for frame k in its camera coordinate system, along with the relative transformation $M_{i \leftarrow k} \in SE(3)$ mapping points from frame k 's coordinate system to that of frame i . Each point $\mathbf{p}_{j'}^{(c)} \in \mathcal{P}_k^{(c)}$ is transformed into the coordinate space of frame i :

$$\mathbf{p}_{j'}^{(c,i \leftarrow k)} = M_{i \leftarrow k} \mathbf{p}_{j'}^{(c)}.$$

These transformed 3D points are then projected onto the image plane of frame i using its intrinsic matrix K_i , yielding reprojected pixel coordinates $\mathbf{x}_{\text{reproj},j'}$. The cross-view reprojection loss between frames i and k is computed as:

$$L_{\text{cross-reproj},i,k} = \frac{1}{M'} \sum_{j'} \|\mathbf{x}_{\text{reproj},j'} - \mathbf{x}_{\text{gtgrid},j'}\|_2^2, \quad (4)$$

Table 1: **Quantitative comparison of video generation models.** We evaluate visual fidelity (FID, FVD), 3D consistency (Warp Error), and novel view synthesis quality (PSNR, SSIM, LPIPS). For these metrics, lower values indicate better performance for FID, FVD, Warp Error, and LPIPS, while higher values are preferable for PSNR and SSIM. Our MarsGen demonstrates state-of-the-art results across all evaluated metrics.

Model	Visual Fidelity		3D Consistency	Novel View Synthesis		
	FID ↓	FVD ↓	Warp Err↓	PSNR ↑	SSIM ↑	LPIPS ↓
<i>Image-to-Video</i>						
Pyramidal-Flow Jin et al. (2024)	78.495	637.952	17.930	—	—	—
CogVideoX Yang et al. (2024)	48.912	411.808	6.866	—	—	—
Kling	74.632	727.130	24.793	—	—	—
Sora Brooks et al. (2024)	142.954	823.418	10707.713	—	—	—
<i>Camera Control Image-to-Video</i>						
CameraCtrl He et al.	123.386	772.476	17.410	20.014	0.441	0.408
ViewCrafter Yu et al. (2024)	169.942	2297.899	501.734	13.143	0.500	0.586
Ours	38.779	364.822	6.071	21.239	0.614	0.351

where M' is the number of points in $\mathcal{P}_k^{(c)}$, and $\mathbf{x}_{\text{grid},j'}$ denotes the expected projection location in frame i (e.g., corresponding to a canonical grid position from frame k). This metric captures how well the geometry inferred from one frame generalizes across viewpoints, revealing discrepancies in spatial alignment and structure.

The overall 2D Warp Error reported is typically an average of these component losses (e.g., $L_{\text{self-avg}}$ and $L_{\text{cross-avg}}$ being the mean self-reprojection and cross-view reprojection errors, respectively) over the sequence or relevant frame pairs:

$$L_{\text{2D-Reproj}} = \frac{1}{2} (L_{\text{self-avg}} + L_{\text{cross-avg}}).$$

A lower reprojection error indicates better geometric consistency.

4 Martian Terrain Video Generator Training

With multimodal M3arsSynth dataset curated by our data engine, we develop and train MarsGen, a conditional generative model for Martian video synthesis. The primary goal of MarsGen is to produce novel, photorealistic video sequences of Martian environments that are not only visually compelling but also exhibit high levels of 3D geometric consistency and physical plausibility. Conditioned on textual prompts or predefined camera trajectories, MarsGen generates temporally coherent RGB sequences that align with the underlying scene structure inferred from the conditioning inputs.

Model Architecture. MarsGen is built upon the Video Diffusion Transformer (VDiT) framework Peebles and Xie (2023). The video and text prompts are first encoded into a latent space Yu et al. (2023); Raffel et al. (2020) and concatenated. A 3D self-attention mechanism, operating across both temporal and spatial dimensions, facilitates a comprehensive interaction between the multimodal information. Finally, a decoder reconstructs the latent representations back into the video space. We train this model on the M3arsSynth dataset to adapt it to the unique visual cues and structural characteristics of Martian environments, thus supporting high-fidelity and controllable video generation under domain-specific constraints.

Controllable Content Generation. To achieve fine-grained control over the generative process, MarsGen incorporates multiple modalities, including a reference initial frame, textual prompts (natural language descriptions), and camera trajectories. These inputs jointly guide the model across spatial, temporal and semantic dimensions. To circumvent the computational demands of full model fine-tuning, we employ a lightweight conditioning strategy inspired by ControlNet architecture Zhang et al. (2023). Specifically, we inject control signals into intermediate layers of the pretrained VDIT backbone, enabling the modulation of generation dynamics without disrupting its learned visual priors.

Video Model Training. We initialize the VDIT backbone with pretrained weights from COGVIDEOX-5B-12V Yu et al. (2023); Yang et al. (2024). We then fine-tune the model, incorporating its controllable branch, on 8 A100 GPUs for 8,000 iterations using the M3arsSynth dataset.

5 Experiments

We evaluate the MarsGen generator, trained on our MarsSynthSim dataset, through comprehensive quantitative and qualitative experiments. This section further compares different reconstruction

Table 2: **Quantitative comparison of reconstruction pipelines for Martian stereo imagery.** We compare COLMAP, the Transformer-based MAST3R Leroy et al. (2024), and our metric-aware initialization method across four key metrics: runtime efficiency (Time), frame-level robustness (Data Utilization), geometric accuracy (2D Reprojection Error Wang et al. (2024a)), and reconstruction density (Point Number). Our pipeline fully utilizes all available data and achieves competitive accuracy, whereas COLMAP fails on nearly 30% of the preprocessed image pairs.

Algorithm	Data Util. (%)	Time (s)	Reproj Err (px) ↓	Point Num
COLMAP Schönberger and Frahm (2016); Schönberger et al. (2016)	71.8	3.6	0.134	~ 2,000
MASt3R Leroy et al. (2024)	100.0	8.7	46.98	~ 250,000
Ours	100.0	8.0	0.77	~ 250,000

methods used in the creation of the MarsSynthSim dataset and presents an ablation study of our M3arsSynth pipeline’s key components, detailing their impacts.

Martian Terrain Video Generation. We quantitatively evaluate the performance of MarsGen, our model fine-tuned on the MarsSynthSim dataset, with a focus on both visual fidelity and 3D geometric consistency. We assess visual quality using FID (Fréchet Inception Distance) Heusel et al. (2017) and FVD (Fréchet Video Distance) Unterthiner et al. (2018), and evaluate geometric consistency through the 2D Warp Error and PSNR. A key capability of MarsGen is its precise camera pose control, which enables us to directly evaluate its novel view synthesis (NVS) performance. Table 1 compares MarsGen against state-of-the-art image-to-video and camera-controlled video generation models. MarsGen consistently outperforms all baselines in terms of visual fidelity, achieving the lowest FID and FVD. In terms of geometric consistency, MarsGen achieves the lowest 2D Warp Error and competitive PSNR, indicating superior preservation of 3D structure during generation. For novel view synthesis, MarsGen also shows superior performance across all metrics, demonstrating the benefit of 3D-aware training on MarsSynthSim. For a qualitative comparison, please see Appendix B. In contrast, general-purpose video models often struggle to maintain consistent spatial geometry under camera motion due to the absence of explicit 3D supervision.

Geometry Initialization Methods. We evaluate alternative approaches for initializing scene geometry within our M3arsSynth pipeline (used to generate the MarsSynthSim dataset), comparing traditional Structure-from-Motion (SfM) pipelines (e.g., COLMAP) and recent transformer-based methods (e.g., MAST3R) against our metric-aware initialization. We use the 2D reprojection error which measures the pixel distance between an observed point in the original image and its corresponding 3D point when re-projected back onto the image using the estimated camera parameters. It thereby jointly assesses the geometric accuracy of the 3D model and the estimated camera pose. Our method combines pre-trained vision foundation models to robustly extract camera and depth priors from challenging Martian stereo imagery. As indicated in Table 2, our pipeline achieves 100% data utilization and reconstructs dense point clouds while maintaining competitive reprojection accuracy and a reasonable runtime. In contrast, COLMAP experiences partial frame failures, and MAST3R, despite generating dense reconstructions, exhibits significant reprojection errors, potentially due to overfitting to unreliable depth priors. Furthermore, we observed that point clouds derived directly from the VGGT model often contain significant artifacts (see Figure 5). We attribute these artifacts to out-of-distribution challenges encountered by the model. Consequently, our reconstruction pipeline utilizes VGGT for intrinsic estimation rather than for direct point cloud export for 3D-GS initialization.

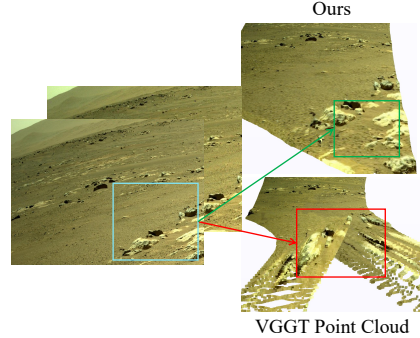


Figure 5: Qualitative comparison of point cloud reconstruction from a Martian input view. Our M3arsSynth engine (top right) produces a coherent point cloud accurately capturing terrain. In contrast, the VGGT Wang et al. (2025b) model (bottom right) exhibits significant misalignment and artifacts.

Ablation Studies. To assess the contribution of individual components within our M3arsSynth reconstruction pipeline, we conduct ablation studies, with results presented in Table 3. Specifically, we evaluate two aspects: (1) the impact of Depth Rescaling, a normalization step designed to align predicted monocular depths with stereo geometry; and (2) the effectiveness of our metric-scale

Table 3: **Ablation study on the core components of the MarsSynthSim reconstruction pipeline.** This study assesses the impact of omitting depth rescaling and replacing our metric-aware initialization with a MAST3R and 3DGS baseline. The findings confirm that both depth normalization and geometric supervision are crucial for high-fidelity, structurally consistent video synthesis.

Depth Rescaling	3D Reconstruction	PSNR \uparrow	SSIM \uparrow	LPIPS \downarrow
\times	Metric-aware Initial	32.20	0.93	0.10
\checkmark	MASt3R Leroy et al. (2024)	28.77	0.59	0.24
\checkmark	Metric-aware Initial	32.73	0.93	0.09

reconstruction pipeline, compared against a variant that initializes geometry using MAST3R with 3DGS for rendering.

The results demonstrate that omitting depth rescaling leads to degraded rendering quality across all metrics, particularly for LPIPS, thereby highlighting the importance of geometric normalization. Furthermore, replacing our metric-scale reconstruction pipeline with the MAST3R + 3DGS baseline results in substantial reductions in both structural similarity (SSIM) and perceptual quality. This outcome underscores the value of our integrated reconstruction strategy, which is crucial for generating datasets that enable consistent and high-fidelity 3D-aware video synthesis.

6 Conclusion, Limitation, and Broader Impact

We introduced M3arsSynth for creating multimodal datasets from sparse rover imagery and MarsGen for generating controllable, photorealistic Martian videos. MarsGen achieves superior visual fidelity and 3D consistency over existing methods, significantly advancing Mars mission simulations for navigation and planning. While our approach significantly supports Mars mission simulation, navigation, and planning through realistic video synthesis, its current limitations include integrating predictive temporal environmental modeling and achieving fine-grained 3D semantic understanding.

Broader Impact. This research significantly enhances Mars mission preparedness by enabling realistic training and system testing through dynamic environmental simulations. However, the underlying generative technology also presents risks such as potential misuse for creating deceptive content, fostering over-reliance on simulations, and concerns regarding resource intensiveness and autonomous system safety.

Acknowledgements

This work was partially supported by Blue Origin and Redwire, as members of the Stanford Center for Aerospace Autonomy Research (CAESAR).

Yue Wang acknowledges generous supports from Toyota Research Institute, Dolby, Google DeepMind, Capital One, Nvidia, and Qualcomm. Yue Wang is also supported by a Powell Research Award.

This research has been supported by computing support on the Vista GPU Cluster through the Center for Generative AI (CGAI) and the Texas Advanced Computing Center (TACC) at the University of Texas at Austin.

References

- Stewart Parker Abercrombie, Alexander Menzies, Alice Winter, Matthew Clausen, Benjamin Duran, Marijke Jorritsma, Charles Goddard, and Alana Lidawer. Onsite: Multi-platform visualization of the surface of mars. In *AGU Fall Meeting Abstracts*, pages ED11C–0134, 2017.
- Sherwin Bahmani, Ivan Skorokhodov, Guocheng Qian, Aliaksandr Siarohin, Willi Menapace, Andrea Tagliasacchi, David B Lindell, and Sergey Tulyakov. Ac3d: Analyzing and improving 3d camera control in video diffusion transformers. *arXiv preprint arXiv:2411.18673*, 2024.
- Raghav Bansal, Gaurav Raj, and Tanupriya Choudhury. Blur image detection using laplacian operator and open-cv. In *2016 International Conference System Modeling & Advancement in Research Trends (SMART)*, pages 63–67. IEEE, 2016.
- Kara H Beaton, Steven P Chappell, Alex Menzies, Victor Luo, So Young Kim-Castet, Dava Newman, Jeffrey Hoffman, Johannes Norheim, Eswar Anandapadmanaban, Stewart P Abercrombie, et al. Mission enhancing

- capabilities for science-driven exploration extravehicular activity derived from the nasa basalt research program. *Planetary and Space Science*, 193:105003, 2020.
- Andreas Blattmann, Tim Dockhorn, Sumith Kulal, Daniel Mendelevitch, Maciej Kilian, Dominik Lorenz, Yam Levi, Zion English, Vikram Voleti, Adam Letts, et al. Stable video diffusion: Scaling latent video diffusion models to large datasets. *arXiv preprint arXiv:2311.15127*, 2023.
- Tim Brooks, Bill Peebles, Connor Holmes, Will DePue, Yufei Guo, Li Jing, David Schnurr, Joe Taylor, Troy Luhman, Eric Luhman, et al. Video generation models as world simulators. *OpenAI Blog*, 1:8, 2024.
- Anpei Chen, Zexiang Xu, Fuqiang Zhao, Xiaoshuai Zhang, Fanbo Xiang, Jingyi Yu, and Hao Su. Mvsnerf: Fast generalizable radiance field reconstruction from multi-view stereo. In *Proceedings of the IEEE/CVF international conference on computer vision*, pages 14124–14133, 2021.
- Guikun Chen and Wenguan Wang. A survey on 3d gaussian splatting. *arXiv preprint arXiv:2401.03890*, 2024.
- Julian Chibane, Aayush Bansal, Verica Lazova, and Gerard Pons-Moll. Stereo radiance fields (srf): Learning view synthesis for sparse views of novel scenes. In *Proceedings of the IEEE/CVF Conference on Computer Vision and Pattern Recognition*, pages 7911–7920, 2021.
- Wenyan Cong, Hanqing Zhu, Kevin Wang, Jiahui Lei, Colton Stearns, Yuanhao Cai, Dilin Wang, Rakesh Ranjan, Matt Feiszli, Leonidas Guibas, et al. Videolifter: Lifting videos to 3d with fast hierarchical stereo alignment. *arXiv preprint arXiv:2501.01949*, 2025.
- Zhiwen Fan, Wenyan Cong, Kairun Wen, Kevin Wang, Jian Zhang, Xinghao Ding, Danfei Xu, Boris Ivanovic, Marco Pavone, Georgios Pavlakos, et al. Instantsplat: Unbounded sparse-view pose-free gaussian splatting in 40 seconds. *arXiv preprint arXiv:2403.20309*, 2(3):4, 2024.
- Yang Gao and Steve Chien. Review on space robotics: Toward top-level science through space exploration. *Science Robotics*, 2(7):eaan5074, 2017.
- Lorenzo Giusti, Josue Garcia, Steven Cozine, Darrick Suen, Christina Nguyen, and Ryan Alimo. Marf: Representing mars as neural radiance fields. In *European Conference on Computer Vision*, pages 53–65. Springer, 2022.
- Benjamin S. Goldstein. Communication from mars: Requirements and limitations. *IEEE Transactions on Aerospace and Electronic Systems*, AES-4(3):392–401, 1968.
- Richard Hartley. *Multiple view geometry in computer vision*. Cambridge university press, 2003.
- Hao He, Yinghao Xu, Yuwei Guo, Gordon Wetzstein, Bo Dai, Hongsheng Li, and Ceyuan Yang. Cameractrl: Enabling camera control for video diffusion models. In *The Thirteenth International Conference on Learning Representations*.
- Hao He, Yinghao Xu, Yuwei Guo, Gordon Wetzstein, Bo Dai, Hongsheng Li, and Ceyuan Yang. Cameractrl: Enabling camera control for text-to-video generation. *arXiv preprint arXiv:2404.02101*, 2024.
- Martin Heusel, Hubert Ramsauer, Thomas Unterthiner, Bernhard Nessler, and Sepp Hochreiter. Gans trained by a two time-scale update rule converge to a local nash equilibrium. *Advances in neural information processing systems*, 30, 2017.
- Mu Hu, Wei Yin, Chi Zhang, Zhipeng Cai, Xiaoxiao Long, Hao Chen, Kaixuan Wang, Gang Yu, Chunhua Shen, and Shaojie Shen. Metric3d v2: A versatile monocular geometric foundation model for zero-shot metric depth and surface normal estimation. *IEEE Transactions on Pattern Analysis and Machine Intelligence*, 2024.
- Binbin Huang, Zehao Yu, Anpei Chen, Andreas Geiger, and Shenghua Gao. 2d gaussian splatting for geometrically accurate radiance fields. In *ACM SIGGRAPH 2024 conference papers*, pages 1–11, 2024.
- Terry Huntsberger, Guillermo Rodriguez, and Paul S Schenker. Robotics challenges for robotic and human mars exploration. In *Robotics 2000*, pages 340–346, 2000.
- A Jain, J Guineau, C Lim, W Lincoln, M Pomerantz, G t Sohl, and R Steele. Roams: Planetary surface rover simulation environment. 2003.
- Wonbong Jang and Lourdes Agapito. Codenerf: Disentangled neural radiance fields for object categories. In *Proceedings of the IEEE/CVF International Conference on Computer Vision*, pages 12949–12958, 2021.
- Yang Jin, Zhicheng Sun, Ningyuan Li, Kun Xu, Hao Jiang, Nan Zhuang, Quzhe Huang, Yang Song, Yadong Mu, and Zhouchen Lin. Pyramidal flow matching for efficient video generative modeling. *arXiv preprint arXiv:2410.05954*, 2024.

- Mohammad Mahdi Johari, Yann Lepoittevin, and François Fleuret. Geonerf: Generalizing nerf with geometry priors. In *Proceedings of the IEEE/CVF Conference on Computer Vision and Pattern Recognition*, pages 18365–18375, 2022.
- Bernhard Kerbl, Georgios Kopanas, Thomas Leimkühler, and George Drettakis. 3d gaussian splatting for real-time radiance field rendering. *ACM Trans. Graph.*, 42(4):139–1, 2023.
- Bernhard Kerbl, Andreas Meuleman, Georgios Kopanas, Michael Wimmer, Alexandre Lanvin, and George Drettakis. A hierarchical 3d gaussian representation for real-time rendering of very large datasets. *ACM Transactions on Graphics (TOG)*, 43(4):1–15, 2024.
- WeiJie Kong, Qi Tian, Zijian Zhang, Rox Min, Zuozhuo Dai, Jin Zhou, Jiangfeng Xiong, Xin Li, Bo Wu, Jianwei Zhang, et al. Hunyuanvideo: A systematic framework for large video generative models. *arXiv preprint arXiv:2412.03603*, 2024.
- Vincent Lepetit, Francesc Moreno-Noguer, and Pascal Fua. Epanp: An accurate $O(n)$ solution to the pnp problem. *International Journal of Computer Vision*, 81(2):155–166, 2009.
- Vincent Leroy, Yohann Cabon, and Jérôme Revaud. Grounding image matching in 3d with mast3r. In *European Conference on Computer Vision*, pages 71–91. Springer, 2024.
- Jiahe Li, Jiawei Zhang, Xiao Bai, Jin Zheng, Xin Ning, Jun Zhou, and Lin Gu. Dngaussian: Optimizing sparse-view 3d gaussian radiance fields with global-local depth normalization. In *Proceedings of the IEEE/CVF conference on computer vision and pattern recognition*, pages 20775–20785, 2024.
- Shiqi Li, Chi Xu, and Ming Xie. A robust $O(n)$ solution to the perspective-n-point problem. *IEEE transactions on pattern analysis and machine intelligence*, 34(7):1444–1450, 2012.
- Hanwen Liang, Junli Cao, Vidit Goel, Guocheng Qian, Sergei Korolev, Demetri Terzopoulos, Konstantinos N Plataniotis, Sergey Tulyakov, and Jian Ren. Wonderland: Navigating 3d scenes from a single image. *arXiv preprint arXiv:2412.12091*, 2024.
- Xinhang Liu, Jiaben Chen, Shiu-Hong Kao, Yu-Wing Tai, and Chi-Keung Tang. Deceptive-nerf/3dgs: Diffusion-generated pseudo-observations for high-quality sparse-view reconstruction. In *European Conference on Computer Vision*, pages 337–355. Springer, 2024.
- Tahir Mahmood, Willis Fulmer, Neelesh Mungoli, Jian Huang, and Aidong Lu. Improving information sharing and collaborative analysis for remote geospatial visualization using mixed reality. In *2019 IEEE International Symposium on Mixed and Augmented Reality (ISMAR)*, pages 236–247. IEEE, 2019.
- Naomi Mathers, Ali Goktogen, John Rankin, and Marion Anderson. Robotic mission to mars: Hands-on, minds-on, web-based learning. *Acta astronautica*, 80:124–131, 2012.
- Michel Maurette. Mars rover autonomous navigation. *Autonomous Robots*, 14(2):199–208, 2003.
- Nargess Memarsadeghi and Amitabh Varshney. Virtual and augmented reality applications in science and engineering. *Computing in Science & Engineering*, 22(3):4–6, 2020.
- Ben Mildenhall, Pratul P Srinivasan, Matthew Tancik, Jonathan T Barron, Ravi Ramamoorthi, and Ren Ng. Nerf: Representing scenes as neural radiance fields for view synthesis. *Communications of the ACM*, 65(1):99–106, 2021.
- OpenAI. Chatgpt-4o, 2024. Accessed: 2025-05-16.
- William Peebles and Saining Xie. Scalable diffusion models with transformers. In *Proceedings of the IEEE/CVF international conference on computer vision*, pages 4195–4205, 2023.
- Alec Radford, Jong Wook Kim, Chris Hallacy, Aditya Ramesh, Gabriel Goh, Sandhini Agarwal, Girish Sastry, Amanda Askell, Pamela Mishkin, Jack Clark, et al. Learning transferable visual models from natural language supervision. In *International conference on machine learning*, pages 8748–8763. PmLR, 2021.
- Colin Raffel, Noam Shazeer, Adam Roberts, Katherine Lee, Sharan Narang, Michael Matena, Yanqi Zhou, Wei Li, and Peter J Liu. Exploring the limits of transfer learning with a unified text-to-text transformer. *Journal of machine learning research*, 21(140):1–67, 2020.
- Tianhe Ren, Shilong Liu, Ailing Zeng, Jing Lin, Kunchang Li, He Cao, Jiayu Chen, Xinyu Huang, Yukang Chen, Feng Yan, et al. Grounded sam: Assembling open-world models for diverse visual tasks. *arXiv preprint arXiv:2401.14159*, 2024.

- Barbara Roessle, Norman Müller, Lorenzo Porzi, Samuel Rota Buló, Peter Kotschieder, and Matthias Nießner. Ganerf: Leveraging discriminators to optimize neural radiance fields. *ACM Transactions on Graphics (TOG)*, 42(6):1–14, 2023.
- Johannes Lutz Schönberger and Jan-Michael Frahm. Structure-from-motion revisited. In *Conference on Computer Vision and Pattern Recognition (CVPR)*, 2016.
- Johannes L. Schonberger and Jan-Michael Frahm. Structure-from-motion revisited. In *Proceedings of the IEEE conference on computer vision and pattern recognition*, pages 4104–4113, 2016.
- Johannes Lutz Schönberger, Enliang Zheng, Marc Pollefeys, and Jan-Michael Frahm. Pixelwise view selection for unstructured multi-view stereo. In *European Conference on Computer Vision (ECCV)*, 2016.
- Seunghyeon Seo, Yeonjin Chang, and Nojun Kwak. Flipnerf: Flipped reflection rays for few-shot novel view synthesis. In *Proceedings of the IEEE/CVF International Conference on Computer Vision*, pages 22883–22893, 2023.
- Xuelun Shen, Zhipeng Cai, Wei Yin, Matthias Müller, Zijun Li, Kaixuan Wang, Xiaozhi Chen, and Cheng Wang. Gim: Learning generalizable image matcher from internet videos. *arXiv preprint arXiv:2402.11095*, 2024.
- Nagabhushan Somraj and Rajiv Soundararajan. Vip-nerf: Visibility prior for sparse input neural radiance fields. In *ACM SIGGRAPH 2023 Conference Proceedings*, pages 1–11, 2023.
- Nagabhushan Somraj, Adithyan Karanayil, and Rajiv Soundararajan. Simplenerf: Regularizing sparse input neural radiance fields with simpler solutions. In *SIGGRAPH Asia 2023 Conference Papers*, pages 1–11, 2023.
- Pengzhi Tian, Meibao Yao, Xueming Xiao, Bo Zheng, Tao Cao, Yurong Xi, Haiqiang Liu, and Hutao Cui. 3d semantic terrain reconstruction of monocular close-up images of martian terrains. *IEEE Transactions on Geoscience and Remote Sensing*, 2024.
- Thomas Unterthiner, Sjoerd Van Steenkiste, Karol Kurach, Raphael Marinier, Marcin Michalski, and Sylvain Gelly. Towards accurate generative models of video: A new metric & challenges. *arXiv preprint arXiv:1812.01717*, 2018.
- Ang Wang, Baole Ai, Bin Wen, Chaojie Mao, Chen-Wei Xie, Di Chen, Fei Wu Yu, Haiming Zhao, Jianxiao Yang, Jianyuan Zeng, et al. Wan: Open and advanced large-scale video generative models. *arXiv preprint arXiv:2503.20314*, 2025a.
- Guangcong Wang, Zhaoxi Chen, Chen Change Loy, and Ziwei Liu. Sparsenerf: Distilling depth ranking for few-shot novel view synthesis. In *Proceedings of the IEEE/CVF international conference on computer vision*, pages 9065–9076, 2023.
- Jianyuan Wang, Nikita Karaev, Christian Rupprecht, and David Novotny. Vggsfm: Visual geometry grounded deep structure from motion. In *Proceedings of the IEEE/CVF conference on computer vision and pattern recognition*, pages 21686–21697, 2024a.
- Jianyuan Wang, Minghao Chen, Nikita Karaev, Andrea Vedaldi, Christian Rupprecht, and David Novotny. Vggt: Visual geometry grounded transformer. *arXiv preprint arXiv:2503.11651*, 2025b.
- Yuehao Wang, Chaoyi Wang, Bingchen Gong, and Tianfan Xue. Bilateral guided radiance field processing. *ACM Transactions on Graphics (TOG)*, 43(4):1–13, 2024b.
- Zhouxia Wang, Ziyang Yuan, Xintao Wang, Yaowei Li, Tianshui Chen, Menghan Xia, Ping Luo, and Ying Shan. Motionctrl: A unified and flexible motion controller for video generation. In *ACM SIGGRAPH 2024 Conference Papers*, pages 1–11, 2024c.
- John Wright, Ashitey Trebi-Ollennu, Frank Hartman, Brian Cooper, Scott Maxwell, Jeng Yen, and Jack Morrison. Terrain modelling for in-situ activity planning and rehearsal for the mars exploration rovers. In *2005 IEEE International Conference on Systems, Man and Cybernetics*, pages 1372–1377. IEEE, 2005.
- Jamie Wynn and Daniyar Turmukhambetov. Diffusionerf: Regularizing neural radiance fields with denoising diffusion models. In *Proceedings of the IEEE/CVF Conference on Computer Vision and Pattern Recognition*, pages 4180–4189, 2023.
- Haolin Xiong. *SparseGS: Real-time 360° sparse view synthesis using Gaussian splatting*. University of California, Los Angeles, 2024.
- Haofei Xu, Songyou Peng, Fangjinhua Wang, Hermann Blum, Daniel Barath, Andreas Geiger, and Marc Pollefeys. Depthspat: Connecting gaussian splatting and depth. In *Proceedings of the Computer Vision and Pattern Recognition Conference*, pages 16453–16463, 2025.

- Zhuoyi Yang, Jiayan Teng, Wendi Zheng, Ming Ding, Shiyu Huang, Jiazheng Xu, Yuanming Yang, Wenyi Hong, Xiaohan Zhang, Guanyu Feng, et al. Cogvideox: Text-to-video diffusion models with an expert transformer. *arXiv preprint arXiv:2408.06072*, 2024.
- Vickie Ye, Ruilong Li, Justin Kerr, Matias Turkulainen, Brent Yi, Zhuoyang Pan, Otto Seiskari, Jianbo Ye, Jeffrey Hu, Matthew Tancik, and Angjoo Kanazawa. gsplat: An open-source library for gaussian splatting. *Journal of Machine Learning Research*, 26(34):1–17, 2025.
- Alex Yu, Vickie Ye, Matthew Tancik, and Angjoo Kanazawa. pixelnerf: Neural radiance fields from one or few images. In *Proceedings of the IEEE/CVF conference on computer vision and pattern recognition*, pages 4578–4587, 2021.
- Lijun Yu, José Lezama, Nitesh B Gundavarapu, Luca Versari, Kihyuk Sohn, David Minnen, Yong Cheng, Vighnesh Birodkar, Agrim Gupta, Xiuye Gu, et al. Language model beats diffusion–tokenizer is key to visual generation. *arXiv preprint arXiv:2310.05737*, 2023.
- Wangbo Yu, Jinbo Xing, Li Yuan, Wenbo Hu, Xiaoyu Li, Zhipeng Huang, Xiangjun Gao, Tien-Tsin Wong, Ying Shan, and Yonghong Tian. Viewcrafter: Taming video diffusion models for high-fidelity novel view synthesis. *arXiv preprint arXiv:2409.02048*, 2024.
- Christoph Zauner. Implementation and benchmarking of perceptual image hash functions. 2010.
- Lvmin Zhang, Anyi Rao, and Maneesh Agrawala. Adding conditional control to text-to-image diffusion models. In *Proceedings of the IEEE/CVF international conference on computer vision*, pages 3836–3847, 2023.
- Zehao Zhu, Zhiwen Fan, Yifan Jiang, and Zhangyang Wang. Fsgs: Real-time few-shot view synthesis using gaussian splatting. In *European conference on computer vision*, pages 145–163. Springer, 2024.

NeurIPS Paper Checklist

1. Claims

Question: Do the main claims made in the abstract and introduction accurately reflect the paper's contributions and scope?

Answer: [\[Yes\]](#)

Justification: The abstract and introduction state the contributions made in the paper.

Guidelines:

- The answer NA means that the abstract and introduction do not include the claims made in the paper.
- The abstract and/or introduction should clearly state the claims made, including the contributions made in the paper and important assumptions and limitations. A No or NA answer to this question will not be perceived well by the reviewers.
- The claims made should match theoretical and experimental results, and reflect how much the results can be expected to generalize to other settings.
- It is fine to include aspirational goals as motivation as long as it is clear that these goals are not attained by the paper.

2. Limitations

Question: Does the paper discuss the limitations of the work performed by the authors?

Answer: [\[Yes\]](#)

Justification: We discuss the limitations in appendix.

Guidelines:

- The answer NA means that the paper has no limitation while the answer No means that the paper has limitations, but those are not discussed in the paper.
- The authors are encouraged to create a separate "Limitations" section in their paper.
- The paper should point out any strong assumptions and how robust the results are to violations of these assumptions (e.g., independence assumptions, noiseless settings, model well-specification, asymptotic approximations only holding locally). The authors should reflect on how these assumptions might be violated in practice and what the implications would be.
- The authors should reflect on the scope of the claims made, e.g., if the approach was only tested on a few datasets or with a few runs. In general, empirical results often depend on implicit assumptions, which should be articulated.
- The authors should reflect on the factors that influence the performance of the approach. For example, a facial recognition algorithm may perform poorly when image resolution is low or images are taken in low lighting. Or a speech-to-text system might not be used reliably to provide closed captions for online lectures because it fails to handle technical jargon.
- The authors should discuss the computational efficiency of the proposed algorithms and how they scale with dataset size.
- If applicable, the authors should discuss possible limitations of their approach to address problems of privacy and fairness.
- While the authors might fear that complete honesty about limitations might be used by reviewers as grounds for rejection, a worse outcome might be that reviewers discover limitations that aren't acknowledged in the paper. The authors should use their best judgment and recognize that individual actions in favor of transparency play an important role in developing norms that preserve the integrity of the community. Reviewers will be specifically instructed to not penalize honesty concerning limitations.

3. Theory assumptions and proofs

Question: For each theoretical result, does the paper provide the full set of assumptions and a complete (and correct) proof?

Answer: [\[NA\]](#)

Justification: The paper does not include theoretical results.

Guidelines:

- The answer NA means that the paper does not include theoretical results.
- All the theorems, formulas, and proofs in the paper should be numbered and cross-referenced.
- All assumptions should be clearly stated or referenced in the statement of any theorems.
- The proofs can either appear in the main paper or the supplemental material, but if they appear in the supplemental material, the authors are encouraged to provide a short proof sketch to provide intuition.
- Inversely, any informal proof provided in the core of the paper should be complemented by formal proofs provided in appendix or supplemental material.
- Theorems and Lemmas that the proof relies upon should be properly referenced.

4. Experimental result reproducibility

Question: Does the paper fully disclose all the information needed to reproduce the main experimental results of the paper to the extent that it affects the main claims and/or conclusions of the paper (regardless of whether the code and data are provided or not)?

Answer: [\[Yes\]](#)

Justification: We fully describe our proposed pipeline, dataset and core building components.

Guidelines:

- The answer NA means that the paper does not include experiments.
- If the paper includes experiments, a No answer to this question will not be perceived well by the reviewers: Making the paper reproducible is important, regardless of whether the code and data are provided or not.
- If the contribution is a dataset and/or model, the authors should describe the steps taken to make their results reproducible or verifiable.
- Depending on the contribution, reproducibility can be accomplished in various ways. For example, if the contribution is a novel architecture, describing the architecture fully might suffice, or if the contribution is a specific model and empirical evaluation, it may be necessary to either make it possible for others to replicate the model with the same dataset, or provide access to the model. In general, releasing code and data is often one good way to accomplish this, but reproducibility can also be provided via detailed instructions for how to replicate the results, access to a hosted model (e.g., in the case of a large language model), releasing of a model checkpoint, or other means that are appropriate to the research performed.
- While NeurIPS does not require releasing code, the conference does require all submissions to provide some reasonable avenue for reproducibility, which may depend on the nature of the contribution. For example
 - (a) If the contribution is primarily a new algorithm, the paper should make it clear how to reproduce that algorithm.
 - (b) If the contribution is primarily a new model architecture, the paper should describe the architecture clearly and fully.
 - (c) If the contribution is a new model (e.g., a large language model), then there should either be a way to access this model for reproducing the results or a way to reproduce the model (e.g., with an open-source dataset or instructions for how to construct the dataset).
 - (d) We recognize that reproducibility may be tricky in some cases, in which case authors are welcome to describe the particular way they provide for reproducibility. In the case of closed-source models, it may be that access to the model is limited in some way (e.g., to registered users), but it should be possible for other researchers to have some path to reproducing or verifying the results.

5. Open access to data and code

Question: Does the paper provide open access to the data and code, with sufficient instructions to faithfully reproduce the main experimental results, as described in supplemental material?

Answer: [No]

Justification: We just promise release our dataset.

Guidelines:

- The answer NA means that paper does not include experiments requiring code.
- Please see the NeurIPS code and data submission guidelines (<https://nips.cc/public/guides/CodeSubmissionPolicy>) for more details.
- While we encourage the release of code and data, we understand that this might not be possible, so “No” is an acceptable answer. Papers cannot be rejected simply for not including code, unless this is central to the contribution (e.g., for a new open-source benchmark).
- The instructions should contain the exact command and environment needed to run to reproduce the results. See the NeurIPS code and data submission guidelines (<https://nips.cc/public/guides/CodeSubmissionPolicy>) for more details.
- The authors should provide instructions on data access and preparation, including how to access the raw data, preprocessed data, intermediate data, and generated data, etc.
- The authors should provide scripts to reproduce all experimental results for the new proposed method and baselines. If only a subset of experiments are reproducible, they should state which ones are omitted from the script and why.
- At submission time, to preserve anonymity, the authors should release anonymized versions (if applicable).
- Providing as much information as possible in supplemental material (appended to the paper) is recommended, but including URLs to data and code is permitted.

6. Experimental setting/details

Question: Does the paper specify all the training and test details (e.g., data splits, hyper-parameters, how they were chosen, type of optimizer, etc.) necessary to understand the results?

Answer: [Yes]

Justification: We include implementation details for our experiments, to a level of detail that is necessary to appreciate the results.

Guidelines:

- The answer NA means that the paper does not include experiments.
- The experimental setting should be presented in the core of the paper to a level of detail that is necessary to appreciate the results and make sense of them.
- The full details can be provided either with the code, in appendix, or as supplemental material.

7. Experiment statistical significance

Question: Does the paper report error bars suitably and correctly defined or other appropriate information about the statistical significance of the experiments?

Answer: [Yes]

Justification: We describe in detail how we obtain quantitative metrics in our experiments.

Guidelines:

- The answer NA means that the paper does not include experiments.
- The authors should answer "Yes" if the results are accompanied by error bars, confidence intervals, or statistical significance tests, at least for the experiments that support the main claims of the paper.
- The factors of variability that the error bars are capturing should be clearly stated (for example, train/test split, initialization, random drawing of some parameter, or overall run with given experimental conditions).
- The method for calculating the error bars should be explained (closed form formula, call to a library function, bootstrap, etc.)
- The assumptions made should be given (e.g., Normally distributed errors).

- It should be clear whether the error bar is the standard deviation or the standard error of the mean.
- It is OK to report 1-sigma error bars, but one should state it. The authors should preferably report a 2-sigma error bar than state that they have a 96% CI, if the hypothesis of Normality of errors is not verified.
- For asymmetric distributions, the authors should be careful not to show in tables or figures symmetric error bars that would yield results that are out of range (e.g. negative error rates).
- If error bars are reported in tables or plots, The authors should explain in the text how they were calculated and reference the corresponding figures or tables in the text.

8. Experiments compute resources

Question: For each experiment, does the paper provide sufficient information on the computer resources (type of compute workers, memory, time of execution) needed to reproduce the experiments?

Answer: [Yes]

Justification: We indicate the type and number of GPUs.

Guidelines:

- The answer NA means that the paper does not include experiments.
- The paper should indicate the type of compute workers CPU or GPU, internal cluster, or cloud provider, including relevant memory and storage.
- The paper should provide the amount of compute required for each of the individual experimental runs as well as estimate the total compute.
- The paper should disclose whether the full research project required more compute than the experiments reported in the paper (e.g., preliminary or failed experiments that didn't make it into the paper).

9. Code of ethics

Question: Does the research conducted in the paper conform, in every respect, with the NeurIPS Code of Ethics <https://neurips.cc/public/EthicsGuidelines>?

Answer: [Yes]

Justification: We conform with the NeurIPS Code of Ethics.

Guidelines:

- The answer NA means that the authors have not reviewed the NeurIPS Code of Ethics.
- If the authors answer No, they should explain the special circumstances that require a deviation from the Code of Ethics.
- The authors should make sure to preserve anonymity (e.g., if there is a special consideration due to laws or regulations in their jurisdiction).

10. Broader impacts

Question: Does the paper discuss both potential positive societal impacts and negative societal impacts of the work performed?

Answer: [Yes]

Justification: We discuss both potential possible societal impacts of the work performed in appendix.

Guidelines:

- The answer NA means that there is no societal impact of the work performed.
- If the authors answer NA or No, they should explain why their work has no societal impact or why the paper does not address societal impact.
- Examples of negative societal impacts include potential malicious or unintended uses (e.g., disinformation, generating fake profiles, surveillance), fairness considerations (e.g., deployment of technologies that could make decisions that unfairly impact specific groups), privacy considerations, and security considerations.

- The conference expects that many papers will be foundational research and not tied to particular applications, let alone deployments. However, if there is a direct path to any negative applications, the authors should point it out. For example, it is legitimate to point out that an improvement in the quality of generative models could be used to generate deepfakes for disinformation. On the other hand, it is not needed to point out that a generic algorithm for optimizing neural networks could enable people to train models that generate Deepfakes faster.
- The authors should consider possible harms that could arise when the technology is being used as intended and functioning correctly, harms that could arise when the technology is being used as intended but gives incorrect results, and harms following from (intentional or unintentional) misuse of the technology.
- If there are negative societal impacts, the authors could also discuss possible mitigation strategies (e.g., gated release of models, providing defenses in addition to attacks, mechanisms for monitoring misuse, mechanisms to monitor how a system learns from feedback over time, improving the efficiency and accessibility of ML).

11. Safeguards

Question: Does the paper describe safeguards that have been put in place for responsible release of data or models that have a high risk for misuse (e.g., pretrained language models, image generators, or scraped datasets)?

Answer: [NA]

Justification: The paper poses no such risks.

Guidelines:

- The answer NA means that the paper poses no such risks.
- Released models that have a high risk for misuse or dual-use should be released with necessary safeguards to allow for controlled use of the model, for example by requiring that users adhere to usage guidelines or restrictions to access the model or implementing safety filters.
- Datasets that have been scraped from the Internet could pose safety risks. The authors should describe how they avoided releasing unsafe images.
- We recognize that providing effective safeguards is challenging, and many papers do not require this, but we encourage authors to take this into account and make a best faith effort.

12. Licenses for existing assets

Question: Are the creators or original owners of assets (e.g., code, data, models), used in the paper, properly credited and are the license and terms of use explicitly mentioned and properly respected?

Answer: [Yes]

Justification: We credit all such assets by appropriate citations and statements.

Guidelines:

- The answer NA means that the paper does not use existing assets.
- The authors should cite the original paper that produced the code package or dataset.
- The authors should state which version of the asset is used and, if possible, include a URL.
- The name of the license (e.g., CC-BY 4.0) should be included for each asset.
- For scraped data from a particular source (e.g., website), the copyright and terms of service of that source should be provided.
- If assets are released, the license, copyright information, and terms of use in the package should be provided. For popular datasets, paperswithcode.com/datasets has curated licenses for some datasets. Their licensing guide can help determine the license of a dataset.
- For existing datasets that are re-packaged, both the original license and the license of the derived asset (if it has changed) should be provided.

- If this information is not available online, the authors are encouraged to reach out to the asset’s creators.

13. **New assets**

Question: Are new assets introduced in the paper well documented and is the documentation provided alongside the assets?

Answer: [\[Yes\]](#)

Justification: We have released the dataset proposed by this paper.

Guidelines:

- The answer NA means that the paper does not release new assets.
- Researchers should communicate the details of the dataset/code/model as part of their submissions via structured templates. This includes details about training, license, limitations, etc.
- The paper should discuss whether and how consent was obtained from people whose asset is used.
- At submission time, remember to anonymize your assets (if applicable). You can either create an anonymized URL or include an anonymized zip file.

14. **Crowdsourcing and research with human subjects**

Question: For crowdsourcing experiments and research with human subjects, does the paper include the full text of instructions given to participants and screenshots, if applicable, as well as details about compensation (if any)?

Answer: [\[NA\]](#)

Justification: The paper does not involve crowdsourcing nor research with human subjects.

Guidelines:

- The answer NA means that the paper does not involve crowdsourcing nor research with human subjects.
- Including this information in the supplemental material is fine, but if the main contribution of the paper involves human subjects, then as much detail as possible should be included in the main paper.
- According to the NeurIPS Code of Ethics, workers involved in data collection, curation, or other labor should be paid at least the minimum wage in the country of the data collector.

15. **Institutional review board (IRB) approvals or equivalent for research with human subjects**

Question: Does the paper describe potential risks incurred by study participants, whether such risks were disclosed to the subjects, and whether Institutional Review Board (IRB) approvals (or an equivalent approval/review based on the requirements of your country or institution) were obtained?

Answer: [\[NA\]](#)

Justification: The paper does not involve crowdsourcing nor research with human subjects.

Guidelines:

- The answer NA means that the paper does not involve crowdsourcing nor research with human subjects.
- Depending on the country in which research is conducted, IRB approval (or equivalent) may be required for any human subjects research. If you obtained IRB approval, you should clearly state this in the paper.
- We recognize that the procedures for this may vary significantly between institutions and locations, and we expect authors to adhere to the NeurIPS Code of Ethics and the guidelines for their institution.
- For initial submissions, do not include any information that would break anonymity (if applicable), such as the institution conducting the review.

16. **Declaration of LLM usage**

Question: Does the paper describe the usage of LLMs if it is an important, original, or non-standard component of the core methods in this research? Note that if the LLM is used only for writing, editing, or formatting purposes and does not impact the core methodology, scientific rigorousness, or originality of the research, declaration is not required.

Answer: [NA]

Justification: The paper does not pose such risks.

Guidelines:

- The answer NA means that the core method development in this research does not involve LLMs as any important, original, or non-standard components.
- Please refer to our LLM policy (<https://neurips.cc/Conferences/2025/LLM>) for what should or should not be described.

A Additional Implementation Details

A.1 Automated Data Filtering Strategies

This subsection details the automated filtering pipeline applied to the raw Martian stereo image pairs obtained from the NASA Planetary Data System (PDS). The following paragraphs describe the specific filtering techniques employed:

Filtering Low-Quality Thumbnails and Grayscale Images. To eliminate uninformative or non-representative visual data, we begin by removing low-resolution thumbnails and grayscale images. This step relies on file-level heuristics including image resolution, file size, and RGB channel statistics. Images with dimensions significantly smaller than our expected minimum resolution or with anomalously small file sizes are classified as thumbnails and excluded. Additionally, we assess the variance across the RGB channels to detect grayscale images; those with minimal inter-channel variance are removed, as they lack the color information necessary for downstream multimodal analysis.

Removing Redundant Content via Perceptual Hashing. To prevent content-level redundancy caused by multiple captures of the same scene under different imaging conditions—such as varied white balance, contrast, or filters—we apply perceptual hashing. This technique generates compact hash codes that encode high-level structural similarity. By computing Hamming distances between these hashes, we identify visually near-duplicate images and discard those exceeding a similarity threshold. This step ensures the dataset maintains semantic diversity and avoids overrepresentation of particular scenes or textures.

Excluding Blurry and Low-Sharpness Images. Maintaining geometric fidelity is critical for tasks such as stereo reconstruction and surface normal estimation. To this end, we apply a sharpness filter using Laplacian variance, a well-established metric that quantifies edge contrast within an image. Frames with a variance below a pre-defined threshold are classified as blurry and automatically excluded. These typically result from motion blur or poor focus, and retaining them would degrade the quality of both photometric and geometric outputs in the synthesized dataset.

Filtering Out Visually Unusable Frames. We analyze the average color intensity histograms of each image to identify those dominated by irrelevant content such as large spacecraft segments, occlusions, or camera malfunctions. These images often display skewed or flat histogram profiles, indicating uniform color patches or unnatural saturation patterns. We flag and remove such frames to ensure that the final dataset primarily comprises clear, terrain-focused scenes with minimal visual obstruction. This enhances the quality and consistency of the data available for learning meaningful Martian representations.

A.2 Implementation of Grounded-SAM-assisted Semi-Automated Data Preprocessing

While the initial automated filtering pipeline, as described in Sec. A.1, addresses common image deficiencies, a subsequent semi-automated refinement stage is crucial for tackling more nuanced and complex visual challenges. These challenges include, but are not limited to, partial occlusions by rover hardware elements (e.g., wheels, antennas, or calibration targets), subtle lens-induced distortions not captured by generic filters.

This refinement phase incorporates a rigorous manual verification protocol for the image set that has passed the initial automated screening. The efficiency and accuracy of this manual review are substantially enhanced by leveraging the capabilities of Grounded-SAM, a sophisticated vision-language segmentation model. Grounded-SAM’s strength lies in its ability to perform open-vocabulary segmentation, identifying and delineating image regions based on arbitrary textual prompts. This is particularly advantageous for our application, as it allows for the flexible identification of diverse and potentially unforeseen rover components or artifacts without requiring model retraining or predefined class lists.

The operational workflow is as follows:

1. **Prompt Formulation:** Human domain experts, familiar with the rover’s morphology and common imaging configurations, formulate targeted textual prompts. These prompts typically reference known spacecraft components that have a high likelihood of intruding

into the image frame (e.g., "rover wheel", "robotic arm telemetry cable", "mast shadow on terrain").

2. **Mask Generation:** Grounded-SAM processes each image in conjunction with these prompts to generate segmentation masks. These masks highlight regions within the image that correspond to the textual descriptions, effectively flagging areas suspected of containing non-terrain elements or problematic features.
3. **Guided Manual Annotation:** The generated masks serve as precise visual guides for human annotators. Instead of scrutinizing the entirety of each image for potential issues, annotators can focus their attention on the regions highlighted by Grounded-SAM. This significantly accelerates the review process and improves the consistency of identifying obscured or compromised data.

Human annotators then perform the critical verification step. Based on the Grounded-SAM-proposed masks and their own expert assessment, they make the final decision to:

- Confirm and accept the mask, leading to the flagging of the highlighted region for exclusion from 3D reconstruction inputs.
- If the segmentation of Grounded-SAM is inaccurate or the image contains unrecognized errors, manual annotation is carried out to obtain a clean image.
- Flag the entire image for exclusion if the problematic regions are too extensive or critical to be simply masked out.

This process ensures that data compromised by non-Martian content or severe artifacts are meticulously identified and appropriately handled.

The direct outcome of this Grounded-SAM assisted semi-automated refinement is a rigorously curated collection of Martian stereo images. These images exhibit high visual integrity, characterized by predominantly unobstructed Martian surfaces, more balanced illumination across the scene, and a minimization of instrumental or environmental artifacts. Such a high-quality, clean dataset forms a reliable and robust foundation essential for the subsequent stages of metric-aware 3D reconstruction and, ultimately, for the training of generative simulation models like MarsGen.

A.3 Details of M3arsSynth construction

The challenge of conversion from CAHVOR to pinhole model This section outlines the conversion from a CAHVOR ($C_{CAHVOR}, A_{CAHVOR}, H_{CAHVOR}, V_{CAHVOR}, O_{CAHVOR}, R_{CAHVOR}$ vectors) camera model to a pinhole model, highlighting the critical parameters and potential impediments. The conversion aims to derive pinhole model parameters (camera center $C_{pinhole}$, rotation matrix R , intrinsic matrix K , and radial distortion coefficients k_0, k_1, k_2) from the CAHVOR parameters.

- **Camera Center:** $C_{pinhole} = C_{CAHVOR}$.
- **Rotation Matrix R :** Derived from normalized horizontal (H_n) and vertical (V_n) vectors, and the optical axis (A_{CAHVOR}).

$$\begin{aligned} H_n &= (H_{CAHVOR} - h_c A_{CAHVOR}) / h_s \\ V_n &= (V_{CAHVOR} - v_c A_{CAHVOR}) / v_s \\ R &= \begin{pmatrix} H_n^T \\ -V_n^T \\ A_{CAHVOR}^T \end{pmatrix} \end{aligned}$$

- **Intrinsic Matrix K :** Determined by focal lengths ($f_u = h_s, f_v = v_s$) and principal point ($c_u = h_c, c_v = v_c$).

$$K = \begin{pmatrix} h_s & 0 & h_c \\ 0 & v_s & v_c \\ 0 & 0 & 1 \end{pmatrix}$$

- **Radial Distortion** k_0, k_1, k_2 : Calculated from \mathbf{R}_{CAHVOR} , with k_1, k_2 also depending on h_s .

$$\begin{aligned} k_0 &= \mathbf{R}_{CAHVOR}[0] \\ k_1 &= \mathbf{R}_{CAHVOR}[1]/(\text{pixel_size} \times h_s)^2 \\ k_2 &= \mathbf{R}_{CAHVOR}[2]/(\text{pixel_size} \times h_s)^4 \end{aligned}$$

The conversion critically depends on four scalar parameters:

- h_s : Horizontal focal length scaling factor.
- v_s : Vertical focal length scaling factor.
- h_c : Horizontal principal point coordinate.
- v_c : Vertical principal point coordinate.

If these four parameters (h_s, v_s, h_c, v_c) are not available, the conversion to a pinhole model is not feasible. Therefore, these four scalar parameters are indispensable for a complete and accurate conversion from the CAHVOR to the pinhole model.

3D Gaussian Splatting for Photorealistic Scene Modeling We details key components and implementation specifics related to our 3D Gaussian Splatting (3DGS) model. The optimization of this model to accurately represent a 3D scene is driven by a combination of two primary loss functions: **Photometric Loss**: This loss ensures that the rendered images from the 3DGS representation closely match the input training images in terms of appearance. It penalizes differences in color and brightness, guiding the optimization towards visual fidelity.

$$\mathcal{L} = (1 - \lambda)\mathcal{L}_1 + \lambda\mathcal{L}_{D\text{-SSIM}} \quad (5)$$

With the goal of guiding the model into plausible geometry, we introduced a geometric prior loss in the process of model optimization, which is **Depth Regularization Loss**. This component utilizes the depth information output by the pre-trained large model and the depth obtained through the rasterization pipeline to supervise the geometric accuracy of the scene.

$$\mathcal{L}_{\text{depth}} = \|D_{\text{render}} - D_{\text{Metric Depth}}^*\|_1 \quad (6)$$

The bilateral grid is a key component in addressing photometric variations and appearance inconsistencies in Martian stereo imagery, which arise from factors like differing camera hardware, lighting conditions, or ISP pipeline transformations. This per-view learnable function transforms the rendered output of a 3DGS model to better match the target image’s appearance. Its implementation involves associating a 3D bilateral grid (a four-dimensional tensor $A \in \mathbb{R}^{W \times H \times D \times 12}$) with each training view, where W, H represent spatial locations, D represents pixel intensity values, and the final dimension stores parameters for a 3×4 affine color transformation matrix. For each rendered pixel, an affine transformation is retrieved via a differentiable slicing operation using trilinear interpolation based on its spatial location and a guidance intensity, allowing the grid’s parameters to be learned end-to-end. Integrated into the 3DGS optimization, the grid processes rendered images before the photometric loss calculation, encouraging it to bridge appearance gaps, and a Total Variation loss is applied as smoothness regularization to prevent overfitting and encourage the modeling of low-frequency changes. The grid’s resolution is typically much smaller than the input images (we have selected here is $16 \times 16 \times 8 \times 12$) to ensure computational efficiency and focus on low-frequency variations, with adaptive sizing possible based on scene characteristics. This joint training approach mitigates appearance inconsistencies, leading to more photorealistic and geometrically consistent 3D scene representations.

Camera Trajectory Synthesis and Motion Description A cornerstone of generating diverse and informative video sequences for the M3arsSynth dataset is the meticulous design and execution of virtual camera trajectories. We begin by defining a repertoire of canonical camera trajectory types. These foundational trajectories, mathematically represented as a sequence of 6-Degrees-of-Freedom (6-DOF) poses $\mathcal{M}_{\text{traj}} = \{(R_t, T_t) \in \text{SE}(3) \mid t = 1, \dots, N\}$, where R_t signifies the camera’s rotation matrix and T_t denotes its translation vector at each discrete timestamp t , are engineered to encompass a wide spectrum of motion profiles. Our trajectory generation process begins by using the two camera poses, solved from the original stereo pair, as start and end keyframes. We then synthesize a variety

of smooth camera paths between these keyframes by applying predefined interpolation methods that follow canonical motion profiles. The spatial extent, or the overall scale and reach, of the predefined canonical trajectories is not fixed; instead, it is dynamically adjusted in response to the specific geometric characteristics of each individual 3D reconstructed Martian scene. This adaptation is primarily driven by the depth information derived from the reconstructed 3D model. Specifically, for regions within a scene that are identified as being in the near-field (characterized by relatively smaller depth values from the camera’s perspective), the corresponding segments of the canonical trajectories are programmatically contracted or scaled down. Conversely, for regions designated as far-field (characterized by significantly larger depth values, indicating distant terrain elements or horizons), the trajectory segments are expanded or scaled up. This depth-adaptive scaling strategy is paramount for ensuring that the synthesized video data effectively and consistently covers the scene’s content at appropriate levels of detail. Following the generation of these adaptively scaled trajectories, the precise 6-DOF pose parameters for each frame serve as the quantitative foundation from which natural language descriptions detailing the camera’s motion characteristics are subsequently derived, forming a key component of the textual modality within the M3arsSynth dataset.

Scene Content Captioning The M3arsSynth dataset incorporates rich textual descriptions to enable and enhance multimodal learning. While depth and normal maps are directly derived from the 3D reconstructed scenes, and camera motion characteristics are derived from the 6-DOF pose parameters of the trajectories, the acquisition of descriptive scene content captions involves a sophisticated process leveraging a Vision Language Model (VLM). We generate scene content captions by applying a VLM, referenced as ChatGPT-4o, to selected views from the synthesized video sequences. Guided by expertise in Martian exploration from our authors, we developed structured prompts for the VLM to ensure high-quality annotations. These prompts include the input image, the classification of the Martian terrain depicted (e.g., "Regolith/Rocky Terrain", "Dunes/Ripples (Sand/Dust)", as shown in Figure 4 of the paper), and a basic descriptive outline of the scene. By conditioning the VLM with this structured input, we obtain detailed and contextually relevant textual descriptions of the visual content. We manually validated a random sample of 20% of the annotations and found no significant errors, which attests to the robustness of our pipeline. This methodology ensures that the textual modality is not only accurate but also aligned with the visual and geometric data, thereby creating a cohesive multimodal dataset suitable for training models like MarsGen for controllable video synthesis.

A.4 MarsGen Architecture and Training Specifics

Conditioning Mechanisms. The MarsGen model integrates multimodal information through distinct conditioning pathways. Textual prompts are initially concatenated with video tokens; this combined representation is then processed through a global attention mechanism to achieve feature fusion. Camera trajectory information is incorporated by first representing camera poses using Plücker embeddings, which are subsequently injected into the model via a ControlNet architecture. Finally, initial video frames are conditioned by concatenating them with the input noise distribution, which then undergoes a denoising process to guide the generation.

Fine-tuning Details. The fine-tuning of MarsGen was conducted with the following hyperparameters. The learning rate was set to 1×10^{-4} . We utilized the AdamW optimizer. A cosine learning rate scheduler was employed, incorporating a warm-up phase. The batch size was configured to 1 per GPU. Training was performed for 8,000 steps, with gradient accumulation implemented over 2 steps.

B Additional Experimental Results and Analysis

B.1 Qualitative Comparisons of Video Generation

The main paper presented quantitative comparisons of our generator against image-to-video and camera-controlled image-to-video models. This appendix provides additional quantitative results against other video generation models. Sora and ViewCrafter, for instance, evidently lack specialized modeling for dynamic Martian scenes, leading to uncontrollable video sequences inconsistent with the theme. This further validates the significance of our proposed dataset.

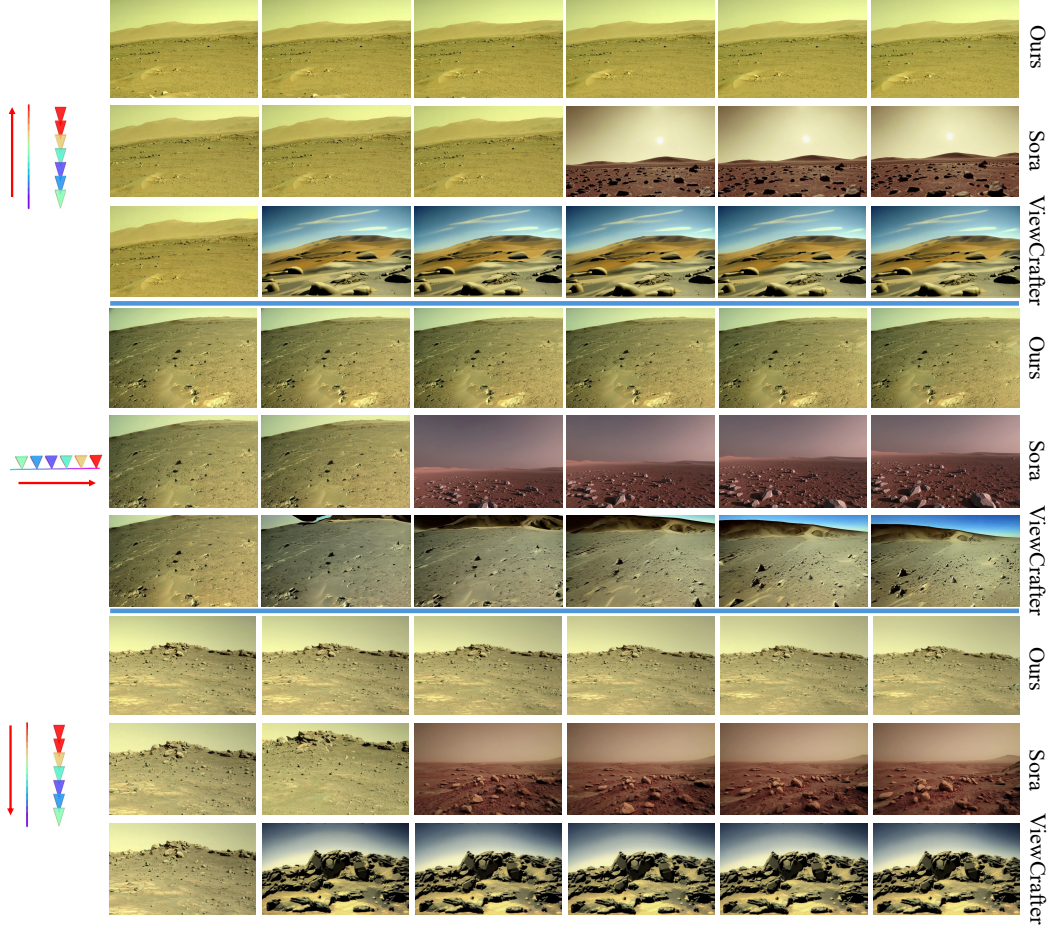


Figure A: **Qualitative comparison of video generation models on dynamic Martian scenes.** Each group of image sequences compares our model against Sora and ViewCrafter under a specific camera control condition. Our model demonstrates improved coherence with the intended camera control and greater thematic consistency for Martian landscapes, whereas Sora and ViewCrafter occasionally produce less controlled or thematically divergent outputs. The relevant comparison video files (in .mp4 format) are located in the corresponding subdirectories under the `comparison/` folder. For example, Sora’s examples are in the `comparison/sora/` directory,

For more comparisons of videos generated by our MarsGen model against the ground truth (GT), please refer to the `ours/` folder. Examples of other models’ failures in generating dynamic Martian scenes can be found in the `others/` folder.

B.2 Qualitative Comparisons of 3D Reconstruction Pipelines

Fig. B illustrates a qualitative comparison of 3D reconstruction outputs from different methodologies when applied to demanding Martian stereo image pairs. The top row of the figure presents results achieved by our M3arsSynth pipeline, which consistently demonstrates the ability to generate coherent and detailed 3D reconstructions of the Martian terrain. These outputs effectively capture the complex geometry and features of the landscape.

In contrast, the second row of Fig. B displays reconstructions produced by the MAST3R pipeline. As indicated by the highlighted regions within the red boxes, MAST3R can encounter difficulties, leading to potential inaccuracies, loss of fine details, or artifacts. While MAST3R achieves 100% data utilization in quantitative assessments, it exhibits a significantly high reprojection error (46.98 px according to Table 2), which may stem from overfitting to unreliable depth priors.

Further highlighting the difficulties faced by existing techniques, traditional Structure-from-Motion (SfM) pipelines like COLMAP demonstrate extremely low utilization and robustness when processing Martian data. For the specific visual examples shown in Fig. B, the COLMAP pipeline failed to generate a usable reconstruction in every instance, indicating its poor suitability for these challenging datasets. This qualitative observation is strongly supported by quantitative data presented in Table 2 of the main paper, which shows that COLMAP experiences failures on nearly 30% of preprocessed Martian image pairs. Such a high failure rate severely restricts its practical application for comprehensive 3D modeling of Martian environments.

In stark contrast, our proposed M3arsSynth pipeline achieves 100% data utilization and successfully reconstructs dense point clouds (averaging 250,000 points) while maintaining a competitive reprojection accuracy (0.77 px, as detailed in Table 2). This robust performance, delivering both high data utilization and superior reconstruction quality, underscores the efficacy of our M3arsSynth data engine in producing the reliable and accurate 3D models that are essential for creating high-fidelity simulations and facilitating advanced video synthesis of Martian terrains.

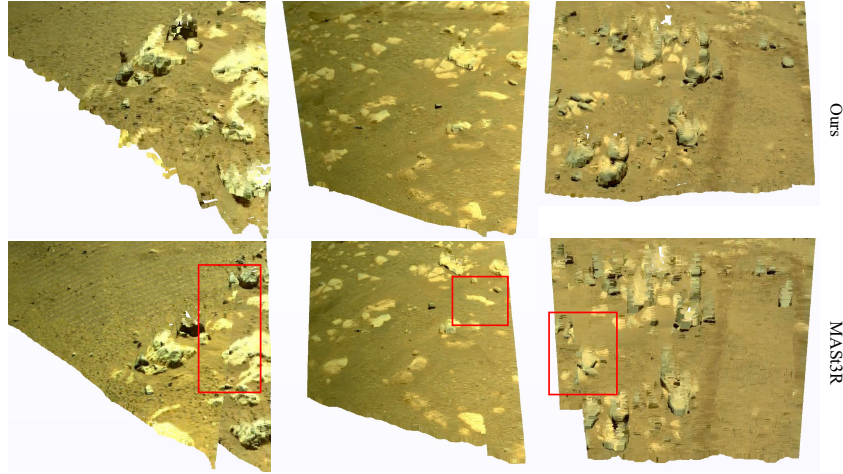


Figure B: **Qualitative comparison of 3D reconstruction pipelines on challenging Martian stereo imagery.** The top row displays reconstructions from our M3arsSynth pipeline, while the bottom row shows results from MASt3R, with red boxes highlighting areas of potential inaccuracy or detail loss. Notably, the COLMAP pipeline failed to produce reconstructions for all depicted examples, underscoring its limitations in robustness and data utilization on Martian datasets.

B.3 Discussion on Geometric Initialization Component Choices

Our experiments, summarized in Table A, validate our component choices for geometric initialization. Our primary goal is accurate, metric-scale reconstruction, which is critical for Martian terrain analysis but not a direct output of methods like VGGT which predicts normalized depth.

The ablation study highlights the limitations of alternatives. The full MASt3R(full) pipeline and its intrinsic estimation (Ours(MASt3R intrin.)) are unstable (46.980 px and 2.016 px, respectively) due to inaccurate 2D correspondences. In contrast, we found VGGT provides more stable intrinsic estimations, likely due to its DINOv2-initialized encoder and normalized training targets.

Furthermore, using VGGT’s outputs directly is suboptimal. Scaling its normalized depth to metric scale (VGGT(metric depth)) is also suboptimal (1.748 px). Using its predicted extrinsics (Ours(VGGT extrin.)) also yields poor results (2.113 px). This is because these non-metric scale poses are fundamentally incompatible with the metric depth priors from Metric3D v2, which are essential to our pipeline. Our approach successfully integrates the strengths of these models while ensuring metric-scale consistency.

Table A: Ablation study on geometric initialization components. Our full method achieves the lowest 2D reprojection error, indicating the most accurate geometric setup.

	MASt3R(full)	VGGT(metric depth)	Ours(MASt3R intrin.)	Ours(VGGT extrin.)	Ours
2D Reproj. ↓	46.980	1.748	2.016	2.113	0.770

B.4 Discussion on Generalization to Lunar and Terrestrial Environments

While our primary motivation stems from Martian exploration, our method is designed for planetary scenes with sparse views and low-texture surfaces. We evaluated our pipeline on similar environments, including public lunar data, performing novel view synthesis from two views.

Furthermore, to test robustness in a general sparse-view context, we performed novel view synthesis on the terrestrial RealEstate10K dataset using only two-view inputs. We benchmarked our approach against Splatt3R and InstantSplat.

The preliminary results, shown in Table B, demonstrate our method’s effectiveness in these challenging sparse-view conditions on both lunar and terrestrial data.

Table B: Sparse-view novel view synthesis benchmarks on Lunar and RealEstate10K data.

Dataset	Method	PSNR ↑	SSIM ↑	LPIPS ↓
Lunar	Ours	29.60	0.920	0.213
RealEstate10K	Splatt3R	15.11	0.492	0.442
	InstantSplat	19.64	0.560	0.291
	Ours	20.81	0.717	0.264